Science Advances
AAAS

Supplementary Materials for

Asynchronous nuclear cycles in multinucleated *Plasmodium falciparum* facilitate rapid proliferation

Severina Klaus, Patrick Binder, Juyeop Kim, Marta Machado, Charlotta Funaya, Violetta Schaaf, Darius Klaschka, Aiste Kudulyte, Marek Cyrklaff, Vibor Laketa, Thomas Höfer, Julien Guizetti, Nils B. Becker, Friedrich Frischknecht, Ulrich S. Schwarz, Markus Ganter*

*Corresponding author. Email: markus.ganter@med.uni-heidelberg.de

Published 30 March 2022, *Sci. Adv.* **8**, eabj5362 (2022)
DOI: 10.1126/sciadv.abj5362

The PDF file includes:

Other Supplementary Material for this manuscript includes the following:

Supplementary Text

Branching process models for nuclear multiplication

General setup: To systematically explore the temporal evolution of nuclear multiplication during schizogony, we construct a mathematical model of nuclear multiplication as a branching process. Within this process, each nuclear cycle is divided into two phases, S and D (fig. S6A). During S-phase the genome is replicated within a single nucleus. The S-phase is followed by two parallel D-phases, one for each daughter nucleus, which comprise the time between the end of DNA replication in the mother and the beginning of the next round of replication in the daughters. Thus, the D-phase in the *i*-th nuclear cycle corresponds to the SD_i and DS_{i+1} phases as defined in the main text.

Each D-phase spans one nuclear division whose exact time is not resolved in the model; instead, we opted for the minimal model that captures individual replications. For simplicity, we model the phase durations as independent random times. This is accurate for adjacent S- and D-phases, as well as D- and next-cycle D-phases, which are not significantly correlated in our data. We also neglect the correlation of S- and subsequent S-phases and between S- and D-phases in sister nuclei (fig. S6C, D). While these were significantly positive in our data, including them had little effect on the predictions of our model, and we therefore do not present these details here. In sum, each (S- or D-) phase duration is independently sampled from a gamma distribution with density, $f(x; \alpha,\beta) = \beta^{\alpha} x^{\alpha-1} e^{-\beta x} / \Gamma(\alpha)$ parameterized by experimental data.

Specifically, realizations of the nuclear branching process are generated as follows. At time $t = 0$ a single nucleus enters S-phase (S_1), with a duration drawn from the corresponding gamma distribution (tab. S1). The two subsequent D-phases ($D_{2,1}$ and $D_{2,2}$) are then sampled independently from the corresponding distribution D_2 (tab. S1). For nuclei of all following generations, this procedure is repeated, the only difference being that the durations for S- and D-phases are somewhat faster (tab. S1). In particular, as cycle phases were measured directly only for the first and second nuclear cycles, we initially adopt the hypothesis that all subsequent nuclear cycles share the statistics of the second cycle.

Stopping the simulation: The branching process ends when a stopping criterion is met. Arguably the simplest criteria are stopping based on elapsed total time, called timer mechanism, or stopping based on total size of the system, called sizer mechanism (*22*, *38*). The timer mechanism predicts no correlation between the duration of the first nuclear cycle and the total time until nuclear multiplication stops, as the total time is determined independently. The sizer mechanism generically produces a positive correlation between the duration of an initial event and the completion of the overall process. If the initial event act as a delay for the complete process, a sizer mechanism moreover predicts a linear relation between initial event time and total time with slope 1; this is because the initial delay results on average in precisely the same delay in completion. For instance, the first nuclear cycle constitutes a pure delay for the completion of nuclear multiplication in an idealized branching process where all sister nuclei are perfectly synchronous. In the present context, the first nuclear cycles are asynchronous. Therefore, the first cycle measured for either sister cell does not simply delay the completion of the full nuclear multiplication process, as the other branch may partially compensate. As a consequence, in this more realistic situation, a regression slope of 1 cannot be expected. Indeed, the data show a linear regression with a smaller slope.

Because our data showed a positive correlation between initial cycle and total replication time (Fig. 4E) we opted for a sizer mechanism. Specifically, we implement the sizer mechanism based on counting of nuclei, and therefore call it a counter mechanism in the following and throughout the main text. After reaching a given number of nuclei n_{stop}, all running DNA replications are completed but no further replications may be initiated. Thus, the final number of nuclei n is given by $n = n_{stop} + n_{running}$, where $n_{running}$ is the number of running replications at the time n_{stop} nuclei are reached.

To parameterize the stopping condition of our branching process, we adjusted n_{stop} to reproduce the total duration of replication. By simulating 10,000 schizogonies with $n_{stop} = 32$, both median and interquartile range of the measured total duration of replication were recovered (fig. S6H). Furthermore, the counter mechanism accurately reproduced the positive correlation and the slope of the linear regression between the first nuclear cycle and the overall time of replication (fig. S6I).

Predictions for the total merozoite count: With the cycling parameters above and $n_{stop} = 32$ the model predicts $n = 39$ (36, 42) [median, (1st, 3rd quartiles)] merozoites in total, whereas 24 (21, 26) were measured (Fig. 4F). As we observed no loss of nuclei that participated in multiplication by time lapse microscopy, this implies that the simulated third and later nuclear cycles are too quick on average. In particular, the assumption of unchanged cycling statistics from the second cycle onwards needed to be revised: cycling speeds up from cycle one to two but then slows down again as schizogony continues.

To estimate the slowdown of nuclear cycling after the second cycle, we modified our previous branching model in a parsimonious way, by introducing one new parameter, the retardation factor γ. In the modified model, starting from the third nuclear cycle, each S- or D-phase is prolonged by a factor of γ per cycle. For example, the S-phase S_4 in cycle $i = 4$ is sampled from a gamma distribution with unchanged $\alpha = 12.49$ (tab. S1) but reduced rate parameter $\beta = \beta/\gamma^{i-2} = \beta/\gamma^2$. Compared to an alternative model where all nuclear cycles $i \geq 3$ are statistically identical and slower than the second cycle, this gradual slowdown has the advantage of avoiding a step-like change in cycling speed.

We then re-fitted the branching process model. 10,000 simulated schizogonies with $\gamma = 1.17$ and $n_{stop} = 17$ show that both median and interquartile range of the total duration of nuclear multiplication (fig. S6H), the final number n of merozoites (Fig. 4F), the positive correlation and the slope of the linear regression (fig. S6I) are captured accurately by the branching process with slowdown. In particular, this model predicts that the final S-phases, which appear in nuclear cycle $i = 5$, are on average 60% longer than S_2.

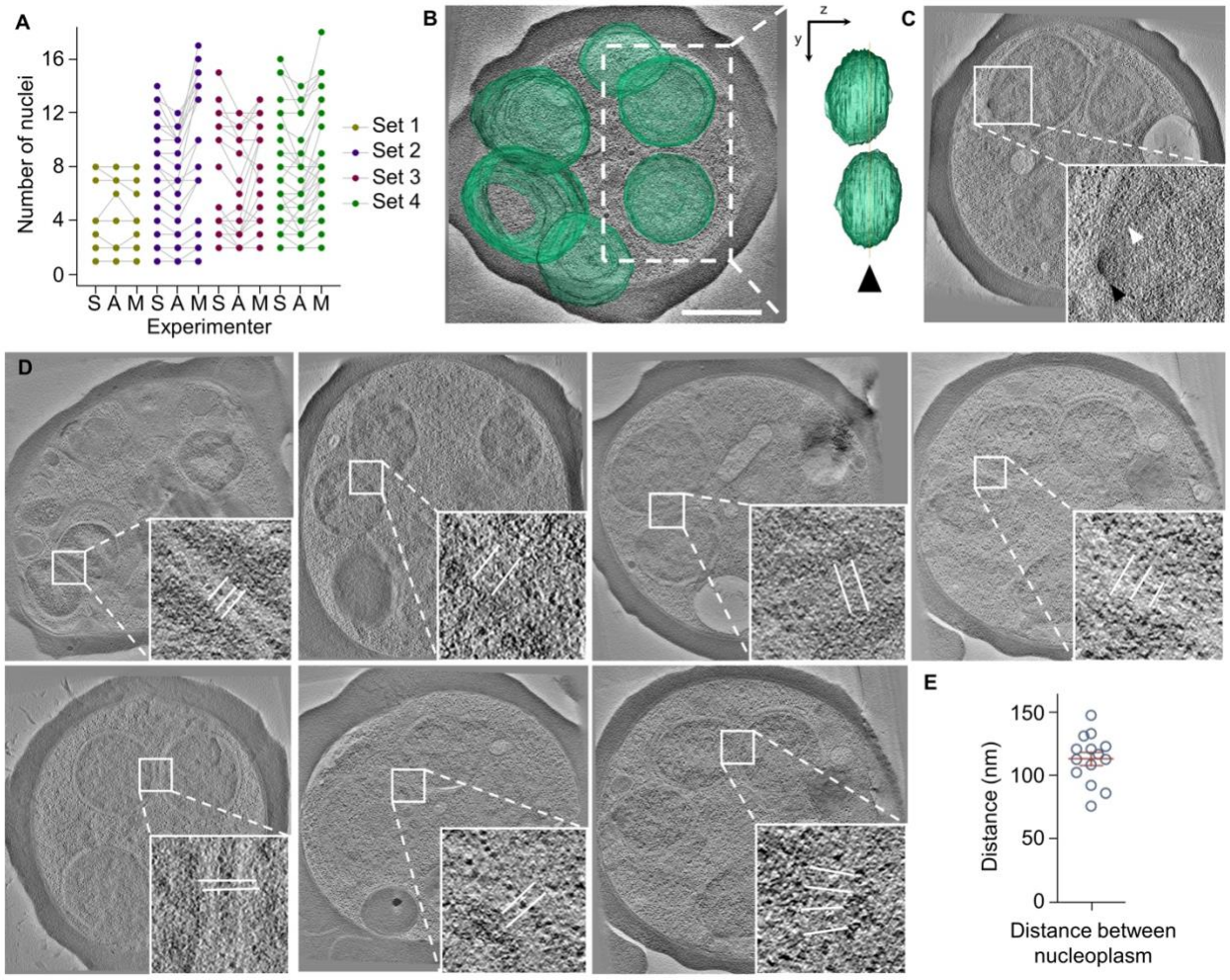

Fig. S1 Nuclei of a *P. falciparum* schizonts are independent cellular compartments except during division. (**A**) Quantification of *P. falciparum* nuclei by three independents experimenters (S, A, and M). Sets of parasites from independent biological replicates. (**B**) Electron tomogram slice, overlayed with the 3D-reconstructed inner nuclear membraned (green) and side view of nuclear volumes showed no connection (90° rotation in x); arrowhead, shown tomogram plane; bar, 1 µm; movie S2. (**C**) Electron tomogram of nucleus undergoing division; white arrowhead, microtubule; black arrowhead, centriolar plaque. (**D**) Measurements of the minimal distance between the nucleoplasm of adjacent nuclei; white lines in inserts, quantified distances; note, ribosomes were detectable in the space between nuclei. (**E**) Average (±standard deviation) minimal distance between the nucleoplasm of adjacent nuclei.

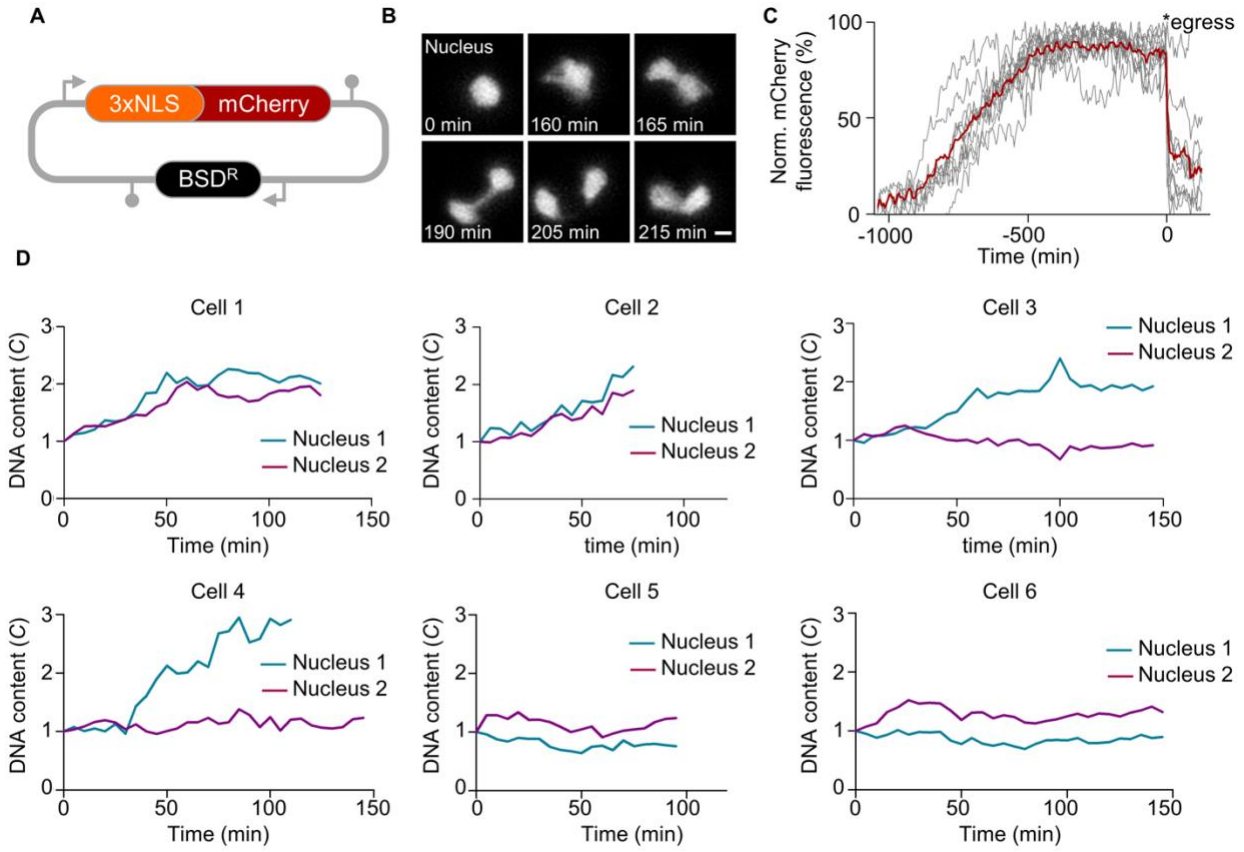

Fig. S2 DNA replication can occur asynchronously in *P. falciparum* nuclei of the same cell. (**A**) Scheme illustrating the plasmid design to generate a reporter parasite with red-fluorescent nuclei. mCherry was N-terminally fused to a triple nuclear localization signal, 3xNLS, and expressed under the control of own promoter and terminator regions. In addition, the plasmid contained a cassette expressing blasticidin-S-deaminase, conferring resistance to blasticidin S (BSD^R); not drawn to scale. (**B**) High-resolution time-lapse microscopy of a nuclear division event, nuclei express 3xNLS::mCherry; bar, 1 µm. (**C**) Long-term time-lapse microscopy of the 3xNLS::mCherry reporter parasite showed that the expression of mCherry is relatively constant for approximately 500 minutes before *P. falciparum* egress, i.e., parasite exit from the host erythrocyte; data from three biological replicates; grey lines, mCherry signal of eleven individual parasites; red line, average. (**D**) Time-lapse microscopy of the 3xNLS::mCherry reporter parasite stained with the DNA dye 5-SiR-Hoechst and quantification of the nuclear DNA content in individual sister nuclei showed asynchronous and synchronous DNA replication events; note, the nuclei of cells 5 and 6 did not replicate during the imaging.

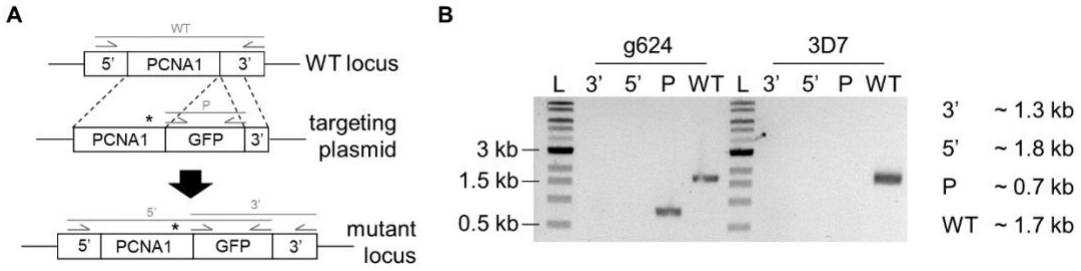

Fig. S3 Endogenous fusion of *P. falciparum* PCNA1 with GFP via genome editing failed. (**A**) Scheme illustrating the CRISPR-based genome editing strategy to fuse endogenous *P. falciparum* PCNA1 with GFP; arrows, primer binding sites; grey lines, expected PCR-amplicons of diagnostic PCR reactions; asterisk, position of mutated PAM-site; not drawn to scale.
(**B**) Diagnostic PCR failed to detect the desired endogenous PCNA1::GFP fusion; note, endogenous tagging was attempted with two different guide RNAs; transfection with guide RNA g738 yielded non-fluorescent parasites; transfection with guide RNA g624 yielded fluorescent parasites; g624, transfectant genomic DNA; 3D7, parental wild type *P. falciparum* genomic DNA; L, 1 kb ladder; 3', 3' test PCR; 5', 5' test PCR; P, plasmid test PCR; WT, wild type test PCR.

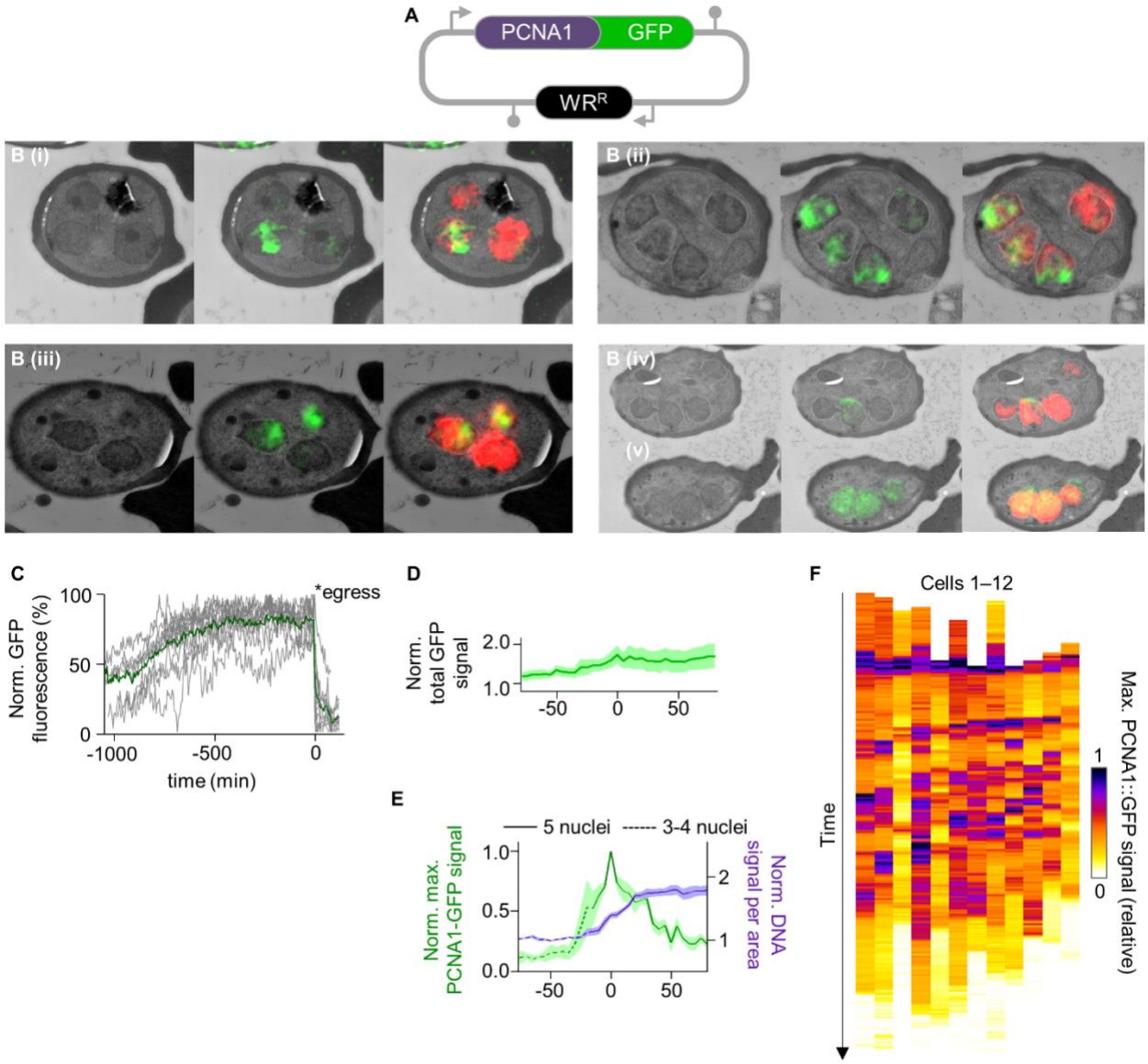

Fig. S4 Characterization of a *P. falciparum* reporter line, episomally expressing PCNA1::GFP and 3xNLS-mCherry. (**A**) Scheme illustrating the plasmid design to generate a reporter parasite for episomal expression of a *P. falciparum* PCNA1::GFP fusion in the 3xNLS::mCherry background. PCNA1::GFP was expressed under the control of own promoter and terminator regions. In addition, the plasmid contained a cassette expressing the human dihydrofolate reductase, conferring resistance to WR99120 (WR^R); not drawn to scale. (**B**) Correlative light and electron microscopy of five *P. falciparum* schizonts (i-v) showed heterogeneous accumulation of PCNA1 among nuclei; left panel, transmission electron micrograph; middle panel, transmission electron micrograph overlayed with GFP signal; right panel, transmission electron micrograph overlayed with GFP and mCherry signal. (**C**) Long-term time-lapse microscopy of the PCNA1::GFP, 3xNLS::mCherry reporter parasite showed that the expression of GFP is relatively constant for approximately 500 minutes before *P. falciparum* egress, i.e., parasite exit from the host erythrocyte; data from three biological replicates; grey lines, GFP signal of eleven individual parasites; green line, average. (**D**) Normalized total PCNA1::GFP signal intensity over 150 minutes, corresponding to Fig. 2C; lines, average (n = 5); bands, standard

deviation. (**E**) Nuclear PCNA1::GFP accumulation caused a peak in the maximal signal intensity, which coincided with a DNA content duplication; solid lines, average; bands, standard deviation; note, data for Fig. 2D were acquired on a Leica SP8 laser scanning confocal microscope and data for fig. S4E were acquired on a PE spinning-disc confocal microscope. (**F**) Normalized maximal PCNA1::GFP-signal intensity over the course of schizogony of twelve individual parasites as proxy for nuclear accumulation of PCNA1. Heatmaps were aligned at the first peak and ordered by the time to second peak.

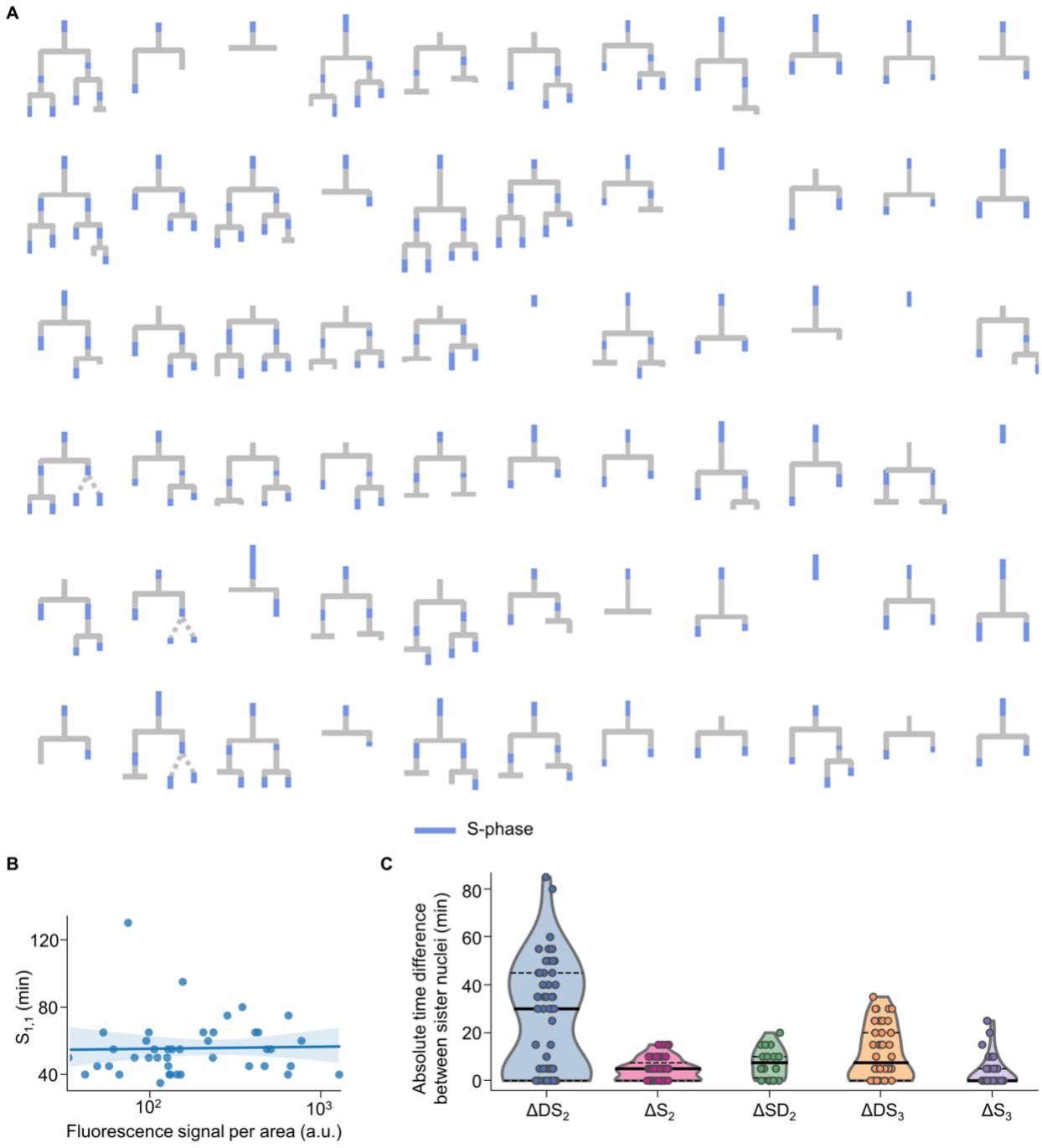

Fig. S5 Overexpression of PCNA1::GFP allows tracing of lineage trees of *P. falciparum* nuclei and does not affect S-phase duration. (**A**) Summary of all lineage trees that were analyzed for Fig. 3B–D, Fig. 4B, E, and Fig. 5B–D; dashed lines, timing of nuclear division event could not be determined with confidence; timing drawn to scale. (**B**) The abundance of episomally expressed PCNA1::GFP did not correlate with the duration of the first S-phase ($S_{1,1}$); a.u., arbitrary units (Spearman's ρ = 0.14, n = 42, p = 0.37). Solid line, linear regression; band, bootstrapped 95% confidence interval. (**C**) Absolute time difference of nuclear cycle phases between sister nuclei

shows that the interval between division and S-phase has the largest influence on synchrony; solid lines, median; dashed lines, quartiles.

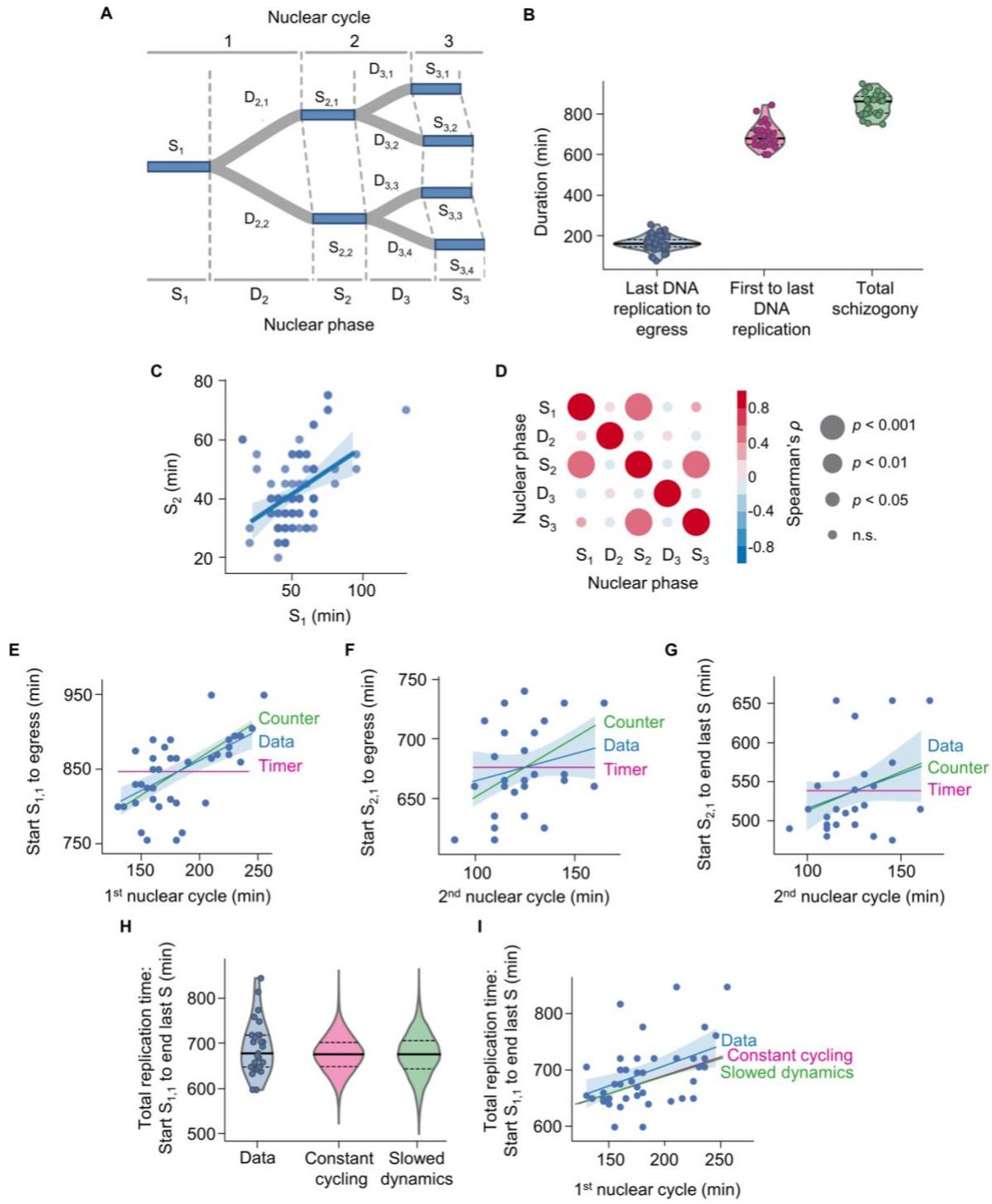

Fig. S6 Parametrization of a mathematical model to simulate nuclear multiplication during *P. falciparum* blood stage schizogony. (**A**) Scheme of the simplified two-phase branching process model. The intervals SD and DS were combined to D; generations of nuclei are indicated above the tree; dashed lines connect the onset and conclusion of S-phases within the generations. (**B**) Quantification of key parameters of *P. falciparum* schizogony via long-term time-lapse microscopy; last DNA replication was defined as last detectable nuclear accumulation of

PCNA1::GFP; solid lines, median; dashed lines, quartiles. (**C**) Duration of the first S-phase (S_1) correlated with the duration of the second S-phase ($S_{2,1}$ and $S_{2,1}$). Solid line, linear regression; band, bootstrapped 95% confidence interval; Spearman's ρ = 0.44, n=85, p = 2.8x10^{-05}. (**D**) Spearman rank correlation of the phases of the two-phase tree. (**E–G**) Live-cell imaging data supports a counter mechanism; solid line, linear regression; band, bootstrapped 95% confidence interval. (**E**) Positive correlation of the duration from the start of S_1 to egress, i.e., parasite exit from the host erythrocyte, with the duration of the first nuclear cycle supports a counter mechanism and contradicts a timer mechanism (Spearman's ρ = 0.55, n = 42, p = 1.9×10^{-4}). (**F**) Correlation of the duration from the start of S_2 to egress with the duration of the second nuclear cycle is consistent with a counter mechanism (ρ = 0.23, n = 35, p = 0.18). (**G**) Correlation of the duration from the start of $S_{2,1}$ to last S-phase with the duration of the second nuclear cycle is consistent with a counter mechanism (ρ = 0.33, n = 35, p = 0.054). (**H**) Time needed to complete nuclear multiplication. Measured data were compared to optimized solutions based on our computational model with independent nuclei and a counter mechanism (with constant cycling-speed or 17% slowdown per nuclear cycle, respectively); solid lines, median; dashed lines, quartiles. (**I**) Simulations of the branching model using a counter stopping criterion (as in the main text, with constant cycling-speed or 17% slowdown per nuclear cycle, respectively) reproduce the positive correlation between duration of first nuclear cycle and the interval from the start of S_1 to last S-phase (observed: ρ = 0.42 [0.15, 0.64]; constant cycling: ρ = 0.55; slowing cycling: ρ = 0.44). They also reproduce the slope m of the linear regression (observed: m = 0.71 [0.26, 1.17]; constant: m = 0.65; slowing: m = 0.60). Solid lines, linear regression; shaded bands and square brackets for m,ρ: bootstrapped 95% confidence intervals.

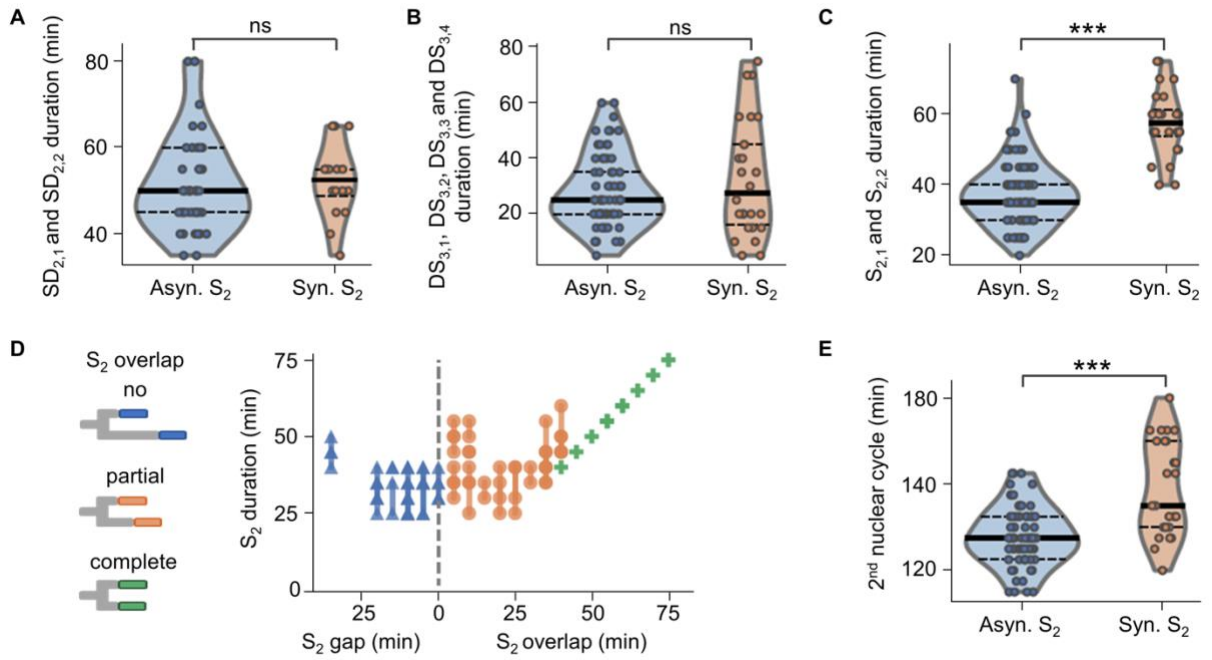

Fig. S7 The effect of synchronous S-phases in sister nuclei. (**A**) The duration from S-phase to division (SD) is indistinguishable in sister nuclei with asynchronous and synchronous S-phases (two-sided Mann-Whitney *U*-test, effective size $f = 0.44$, $n_1 = 44$, $n_2 = 16$, $p = 0.47$. (**B**) The duration from division to S-phase (DS) is indistinguishable in sister nuclei with synchronous and asynchronous S-phases ($f = 0.44$, $n_1 = 65$, $n_2 = 26$, $p = 0.68$). (**C**) Synchronous S-phases in pairs of sister nuclei are significantly longer ($f = 0.065$, $n_1 = 93$, $n_2 = 24$, $p = 3.4\times10^{-11}$). (**D**) The duration of S-phases in pairs of sister nuclei (vertical lines) versus the temporal gap or overlap between S-phases. Asyn., asynchronous; syn., synchronous. (**E**) The 2nd nuclear cycle is significantly longer in pairs of sister nuclei with synchronous S-phases ($f = 0.22$, $n_1 = 64$, $n_2 = 26$, $p = 2.4\times10^{-5}$). Solid lines, median; dashed lines, quartiles.

Table S1. Parameters used in the branching process models.

	First nuclear cycle		Second and higher nuclear cycle	
Nuclear cycle phase	S_1	D_1	$S_{>1}$	$D_{>1}$
Input data	S_1	SD_1+$DS_{2,1}$, SD_1+$DS_{2,2}$	$S_{2,1}$, $S_{2,2}$	$SD_{2,1}$ + $DS_{3,1}$, $SD_{2,1}$ + $DS_{3,2}$, $SD_{2,2}$ + $DS_{3,3}$, $SD_{2,2}$ + $DS_{3,4}$
α	8.14	18.77	12.49	25.85
β	0.15	0.15	0.30	0.32
KS test *p*	0.24	0.033	0.013	0.17

Parameters of the gamma distribution used in the branching process models, based on time-lapse microscopy of the initial nuclear cycles. The shape and rate parameter of the gamma distributions, α and β, were estimated by maximizing a log-likelihood function. The KS test is performed as a one-sample test with a two-sided alternative hypothesis.

Movie S1.

Sections of an electron tomogram of a high-pressure frozen multinucleated *P. falciparum* blood-stage parasite; resolution reduced by a factor of 4; every 4th slice is shown; brightness and contrast adjusted for better visibility; bar, 1 µm.

Movie S2.

Sections of an electron tomogram of a high-pressure frozen multinucleated *P. falciparum* blood-stage parasite; resolution reduced by a factor of 4; every 8th slice is shown; brightness and contrast adjusted for better visibility; bar, 1 µm.

Movie S3.

Time-lapse microscopy of a reporter parasite expressing nuclear mCherry (magenta) and stained with the DNA dye 5-SiR-Hoechst (multicolor); DIC image, single slice; fluorescent images, z-projection of 9 z-slices; brightness and contrast adjusted for better visibility; bar, 2 µm.

Movie S4.

Time-lapse microscopy of a reporter parasite expressing nuclear mCherry (magenta) and PCNA1::GFP (green); images, z-projection of 17 slices; brightness and contrast adjusted for better visibility; bar, 2 µm.

Movie S5.

Time-lapse microscopy of a reporter parasite expressing nuclear mCherry (magenta) and PCNA1::GFP (green); images, z-projection of 17 slices; brightness and contrast adjusted for better visibility; bar, 2 µm.

Movie S6.

Time-lapse microscopy of a reporter parasite expressing nuclear mCherry (magenta) and PCNA1::GFP (green) showing synchronous S-phases (i.e. nuclear accumulation of PCNA1::GFP); images, z-projection of 17 slices; brightness and contrast adjusted for better visibility; bar, 2 µm.